JOURNAL OF THEORETICAL AND APPLIED MECHANICS
44, 3, pp. 533-552, Warsaw 2006

MICROSTRUCTURAL EFFECTS ON DAMAGE IN COMPOSITES – COMPUTATIONAL ANALYSIS

Leon Mishnaevsky Jr.

University of Stuttgart, IMWF and
Darmstadt University of Technology, Institute of Mechanics, Germany
e-mail: mishnaevsky@web.de

In this paper, microstructural effects on the damage resistance of composite materials are studied numerically using methods of computational mesomechanics of materials and virtual experiments. Several methods and programs for automatic generation of 3D microstructural models of composites based on the geometrical description of microstructures as well as on the voxel array data have been developed and tested. 3D FE (Finite Element) simulations of the deformation and damage evolution in particle reinforced composites are carried out for different microstructures of the composites. Some recommendations for the improvement of the damage resistance of lightweight metal matrix composites with ceramic reinforcements are obtained.

Key words: damage, composite, finite elements, micromechanics, numerical simulations

1. Introduction

The optimal design of particle-reinforced materials on the basis of computational simulations of their behaviour has attracted growing interest of researchers over the last two decades (Mishnaevsky and Schmauder, 2001). One of the ways to determine the optimal microstructures is to use numerical (micro- and mesomechanical) simulations of deformation and failure processes in the materials, and to carry out the "virtual testing" of different microstructures of materials.

According to Mishnaevsky (1998), Mishnaevsky and Schmauder (2001), Mishnaevsky *et al.* (2003a, 2004b), a possible scheme of the optimiza-

tion/design of materials on the basis of numerical experiments should include the following steps:

- Problem definition: definition of necessary properties to be improved on the basis of the analysis of service conditions and the analysis of the available means of the microstructure control; analysis of the effects of the material manufacturing and processing on the microstructures of materials (examples: effect of duration and temperature of sintering on grain sizes and contiguity of hard alloys; effect of hot working on the type of structures in high speed steel)
- Analysis of real microstructures of considered materials (digitizing micrographs from cuts of materials, image analysis of the material structure, search for regularities or periodicity in the microstructures) (Mishnaevsky *et al.*, 2003a; Wulf, 1995; Wulf *et al.*, 1993)
- Choice of the appropriate simulation approach: unit cell approach (for regular microstructures) or real structure simulation, cohesive models of fracture, element elimination method, etc. (Mishnaevsky, 1998; Mishnaevsky and Schmauder, 2001; Mishnaevsky *et al.*, 2003a, 2004b)
- Experimental determination of mechanical properties, damage mechanisms (debonding, particle failure, etc.) and failure conditions for constituents of the material to be optimized (Mishnaevsky *et al.*, 1999b, 2003b)
- Development of numerical models of the material with real microstructures and verification of the model by comparing the calculated and experimental results (Wulf, 1995; Wulf *et al.*, 1993)
- Virtual (computational) testing of ideal artificial microstructures (Mishnaevsky, 2004, 2005; *et al.* Mishnaevsky *et al.*, 1999a, 2004a); optimization of microstructures; comparison and recommendations for the improvement of the microstructures of materials. By testing some typical idealized microstructures of a considered material in numerical experiments, one determines the directions of the material optimization and preferable microstructures of materials under given service conditions. Such simulations should be carried out for the same loading conditions and material as the real structure simulations, which proved to reflect adequately the material behaviour
- Realization of the recommended microstructures in cooperation with industry, using powder metallurgy technology, etc.; verification of results.

The main subject of this work is the development of numerical tools for the computational mesomechanical testing of materials and carrying out numerical

experiments, which should lead to the development of recommendations for the improvement of material structures.

2. Automatic generation of microstructural 3D models of composite materials

The concept of the optimal design of materials on the basis of numerical testing of microstructures can be realized if big series of numerical experiments for different materials and microstructures can be carried out quickly, in a systematic way, automatically. This can be done if the labour costs of the numerical experiments, a significant part of which are the efforts of the generation of micromechanical models, are kept very low. To achieve this, a series of programs was developed, which should automate the step of generation of 3D microstructural models of materials. After a 3D microstructural model of a material with a complex microstructure is generated, the numerical testing of the microstructure is carried out with the use of commercial finite element software. In this Section, we present several newly developed programs for the automatic generation of 3D microstructural models of heterogeneous materials.

2.1. Programm "Meso3D" for automatic geometry-based generation of 3D FE microstructural models

To simplify and automate the generation of 3D FE microstructural models of materials, the program "Meso3D" was developed (Mishnaevsky, 2004; Mishnaevsky *et al.*, 2004a).

The program defines geometry, mesh parameters and boundary conditions of different multiparticle unit cell models of materials, and generates a command file (session file) for the commercial FE Pre- and Post-Processing software MSC/PATRAN, which creates automatically a multiparticle unit cell model of a representative volume of a composite material. During the model generation controlled by the command file, the geometry of the cell is created as a box containing a given amount of round or ellipsoidal particles of different sizes. Both embedded and non-embedded unit cells can be produced. Then, the designed microstructures (matrix and particles) are meshed with tetrahedral elements using the free meshing technique (Mishnaevsky, 2004). After that, the mesh is automatically improved, and finally the boundary conditions and material properties are defined. The model can be further changed

or run at different commercial or non-commercial FE programs (as ABAQUS, NASTRAN, etc.).

The geometry and parameters of the unit cell are defined during a short interactive session, in which the parameters are introduced into the program either directly or by multiple choice. The microstructures to be generated are defined by the sizes of the considered cell, shape, volume content and amount of inclusions, kind of the inclusion distribution (random, pre-defined, clustered, graded, etc.), probability distribution of the inclusion sizes, etc. The model is defined by the fineness of the meshing, availability or non-availability and sizes of embedding, boundary conditions (uniaxial tension or triaxial loading). Due to the fact that the models are *geometry-based*, only rather simple shapes of the inclusions (round and ellipsoidal) can be taken into account in this model.

The radii, form and positions of the inclusions can be read from the input text file (for the cases of pre-defined or regular particle arrangements), or generated with the use of a random number generator. In the second case, there are options of the random, clustered, gradient arrangements or dense packing of particles.

FE models of both artificial and real microstructures can be generated with this program. In the case of real microstructures, either experimentally determined coordinates and radii of inclusions are given in the input file, or experimentally determined probability distributions of these values can be used to generate quasi-real microstructures.

For generation of different artificial microstructures and particle arrangements as well as for statistical analysis of the generated microstructures, several subroutines were used. In the case of generation of random particles arrangement using a uniform random number generator, each coordinate is produced independently, with another random number seed. After the coordinates of the first particle are defined, the coordinates of each new particle are determined both by using the random number generator and from the condition that the distance between the new particle and all available particles is no less than 0.1 of the given particle radius. If the condition is not met, the seed of the random number generator is changed, and the coordinates of the new particle are determined anew. In order to avoid the boundary effects, the distance between a particle and the borders of the box is set to be no less than 0.05 of the particle radius.

In order to generate localized particle arrangements, like clustered, layered and gradient particle arrangements, the coordinates of particle centers were calculated as random values distributed by the Gauss law. The mean values of the corresponding normal distribution of the coordinates of particle centers

were assumed to be the coordinates of a center of a cluster (for the clustered structure), or the Y- or Z-coordinate of the border of the box (for the gradient microstructures). The standard deviations of the distribution can be varied, which allows one to generate different particle arrangements, from highly clustered or highly gradient arrangements (very small deviation) to fast uniformly random particle arrangements (a deviation comparable with the box size).

Another procedure is used to create multiparticle unit cells with a high volume content of particles. In this case, a dense packing algorithm is used. First, the average distance between particle centers is determined from the required volume content of particles and their amount. Then, the unit cell is filled by the particles "layer after layer". With this procedure, the volume content of particles of about 40% can be achieved.

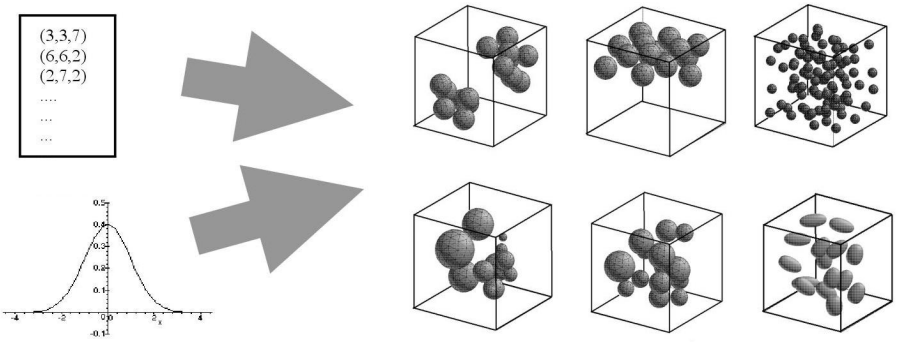

Fig. 1. Schema of the program "Meso3D" and examples of 3D microstrucural models of representative volumes of materials generated with the model (Mishnaevsky, 2004)

2.2. Program "Voxel2FEM" for the voxel array based generation of 3D microstructural models

The geometry-based approach to the description of inclusion shapes, realized in the program "Meso3D", works well only for relatively simple geometrical forms of microstructural elements in a composite (like round or ellipsoidal inclusions). This can be considered as a general drawback of many methods of 3D modelling of microstructures: both shapes of inclusions and their spatial distribution are often oversimplified.

To automate the generation and meshing of 3D FE Models of materials with complex microstructures, the program "Voxel2FEM", which allows one to avoid this drawback, was developed (Mishnaevsky, 2005). The program produces interactively a command file, which generates 3D FE microstructural mo-

dels of representative volumes of a material. In the framework of the program, the information about the spatial distribution of phases in the representative volume is presented as a voxel array. The material volume is presented as an $N \times N \times N$ array of points (voxels), each of them either black (0) or white (1) (for a two-phase material). A generalization of this approach for a multiphase material can be simply done. The voxel array data can be either read from an input file (real microstructure case) or generated in the program by using the random number generator. The program can generate also voxel arrays for different arrangements of round particles in a matrix (multiparticle unit cell). On the basis of voxel arrays, the program "Voxel2FEM" generates 3D microstructural models of the representative material volume. Figure 2 shows examples of the generated models (Mishnaevsky, 2005).

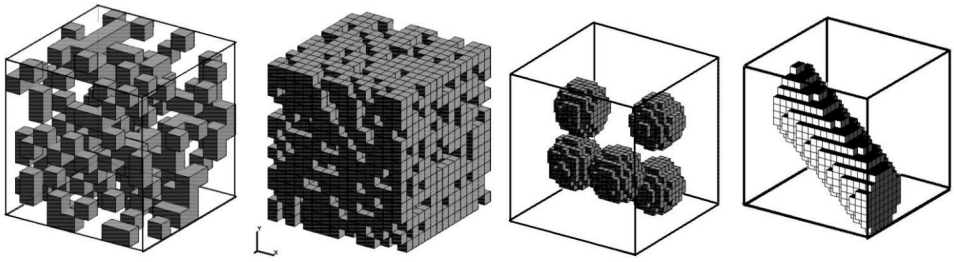

Fig. 2. 3D FE microstructural models generated with the use of the program "Voxel2FEM": a porous material, multiparticle unit cell model of a composite, a cell with the inclined fiber

2.3. Routine for damage simulation

In this Section, a newly developed ABAQUS subroutine for the damage modeling in Al/SiC composites is presented. The micromechanisms of damage evolution in most Al/SiC composites under mechanical loading can be described as follows: first, some particles become damaged and fail (in the case of relatively large particles) or debond from the matrix (for smaller particles); after that cavities and voids nucleate in the matrix (initially, near the broken particle), grow and coalesce, and that leads to the failure of the matrix ligaments between particles and finally to formation of a macrocrack in the volume Mummery and Derby (1993), Derrien *et al.* (1999). According to Mummery and Derby (1993), the interface debonding becomes one of the main damage mechanisms in the case of relatively small particles ($\sim< 10\mu$m), but does not play the leading role in the case of bigger particles.

Wulf (1995) studied experimentally and numerically the damage growth and fracture in real microstructures of Al/SiC composites. According to Wulf (1995), finite-element simulations with the damage parameter based on the model of spherical void growth in a plastic material in a general remote stress field with high stress triaxiality, developed by Rice and Tracey (1969) produced excellent results for Al/SiC composites: both crack paths in a real microstructure of a material and force-displacement curves were practically identical in experiments and simulations. The damage parameter, considered by Wulf, is determined by integrating the incremental damage indicator, which is defined as an increment of the plastic strain divided by the reference failure strain (which is determined as a value inversely proportional to the void growth velocity) (Mishnaevsky *et al.*, 1999a; Wulf *et al.*, 1993). In our simulations, the Rice-Tracey damage indicator was used as a parameter of the void growth in the Al matrix.

To model the damage and local failure of SiC particle, the criterion of critical maximum principal stress in the particle material was used. According to Derrien *et al.* (1999), the SiC particles in Al/SiC composites become damaged and ultimately fail when the critical maximum principal stress in a particle exceeds 1500 MPa. This value was used in our simulations as a criterion of damage of SiC particles as well.

An the ABAQUS Subroutine USDFLD, which calculates the Rice-Tracey damage indicator in the matrix and the maximum principal stress in particles, and allows one to visualize the damage (microcrack and void) distribution in the material was developed. The damage was modeled as a local weakening of finite elements in which the damage criterion exceeded the critical value (Mishnaevsky *et al.*, 2003a). After an element failed, the Young modulus of this element was set to a very low value (50 Pa, i.e., about 0.00001% of the initial value).

2.4. Comparison of the geometry-based and the voxel array based methods of generation of 3D FE models

The program "Voxel2FEM" and the voxel array based method of reconstruction of 3D microstructures were tested by carrying out FE simulation of deformation and damage in composite unit cells with an identical ideal 3D microstructure, generated with the use of the programs "Meso3D" and "Voxel2FEM" and comparing the results of simulations.

The multiparticle unit cells ($10 \times 10 \times 10$ mm) with 5 round particles was considered in both cases. The considered material was Al matrix reinforced by SiC particles (volume content 5%).

The SiC particles behaved as elastic isotropic damageable solids, characterized by Young's modulus $E_P = 485\,\text{GPa}$, Poisson's ratio 0.165 and the local damage criterion, discussed below. The Al matrix was modeled as an isotropic elasto-plastic solid, with Young's modulus $E_M = 73\,\text{GPa}$, and Poisson's ratio 0.345. The experimental stress-strain curve for the Al matrix was taken from Mishnaevsky (2004), Mishnaevsky *et al.* (2004a). When approximating the experimental stress-strain curve by the deformation theory, tjhe flow relation (Ludwik hardening law) is $\sigma_y = \sigma_{yn} + h\varepsilon_{pl}^n$, where σ_y denotes the actual flow stress, σ_{yn} – initial yield stress, and ε_{pl} – accumulated equivalent plastic strain, h and n – hardening coefficient and hardening exponent. The parameters of the curve are as follows: $\sigma_{yn} = 205\,\text{MPa}$, $h = 457\,\text{MPa}$, $n = 0.20$.

As output parameters of the numerical testing of microstructures, the effective response of materials and the amount of failed particles N_F versus the far-field strain curves were considered.

Totally, the geometry-based model contained about 30000 elements, and the voxel based model 8000 brick elements. Each particle contained about 400 finite elements in the geometry-based model, and 80 elements in the voxel-based model.

The nodes at the upper surface of the box were connected, and the displacement was applied to one node only. The model was subject to the uniaxial tensile displacement loading, 2.0 mm. The uniaxial tensile response of each microstructure was computed by the finite element method. The simulations were done with the ABAQUS/Standard.

Figure 3b shows the considered cells as well as the stress-strain curves and the fraction of failed elements versus applied strain curves obtained numerically. One can see that the obtained results are very close: the stress-strain curves differ only by 4%. The functions of the fraction of failed particles versus the applied strain, obtained in the simulations, are very close as well.

3. Numerical experiments: effect of microstruxcuture of composites on damage resistance

3.1. Effect of particle arrangement of damage resistance

In this part of the work, the effect of particles arrangement on the deformation and damage evolution in the composite were considered, using the program "Meso3D". The mechanical behaviour and damage evolution in the materials with different (artificially designed) microstructures were simulated,

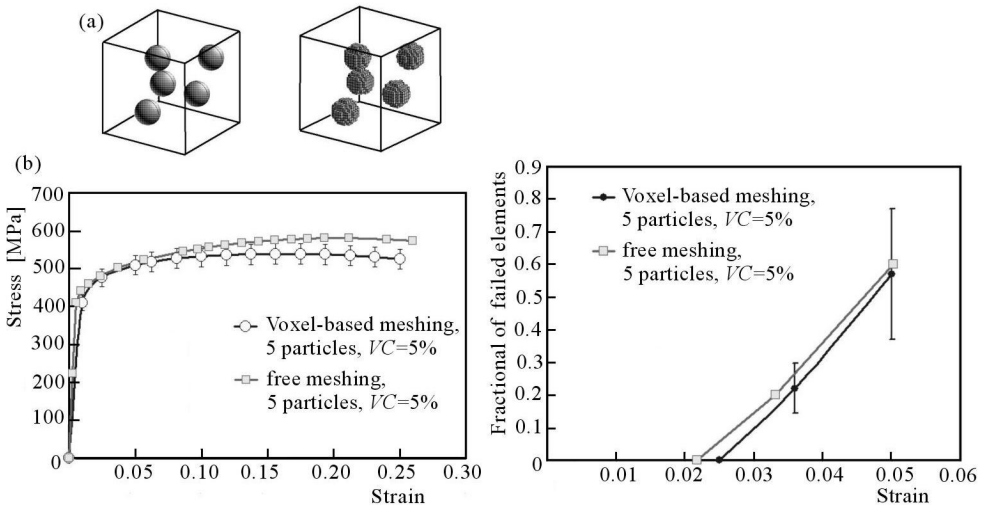

Fig. 3. 3D unit cells (a) and comparison of simulations in the framework of geometry-based and voxel array based approaches (b) (Mishnaevsky, 2005)

and the amount of failed particles and tensile stress-strain curves for each microstructures determined.

Figure 1 gives examples of random, regular, clustered, and highly gradient arrangements of particles, considered in the simulations. Two types of gradient particle arrangements were considered: an arrangement of a particle with the vector of gradient (from low to high particle concentration region) coinciding with the loading direction (called in the following the "gradient Y" microstructure), and a microstructure with the gradient vector perpendicular to the loading vector (called in the following the "gradient Z" microstructure). The standard deviations of the normal distribution of the Y or Z coordinates of particle centers (for the Y and Z gradient microstructures, respectively) were taken 2 mm, what ensured rather high degree of gradient. The same standard deviations were taken for the clustered particle arrangements.

Figure 4 shows tensile stress-strain curves and the amount of failed particles in the box plotted versus the far-field strain for random, regular, clustered and gradient microstructures (for 15 particles, $VC = 10\%$). Figure 5 gives distributions of equivalent plastic strains on the particle/matrix interfaces and in a vertical section in the microstructures with random particle arrangements (15 particles, $VC = 10\%$).

It can be seen in Fig. 4 that the particle arrangement hardly influences the effective response of the material in the elastic area or at small plastic deformation. The influence of the type of particle arrangement on the effective

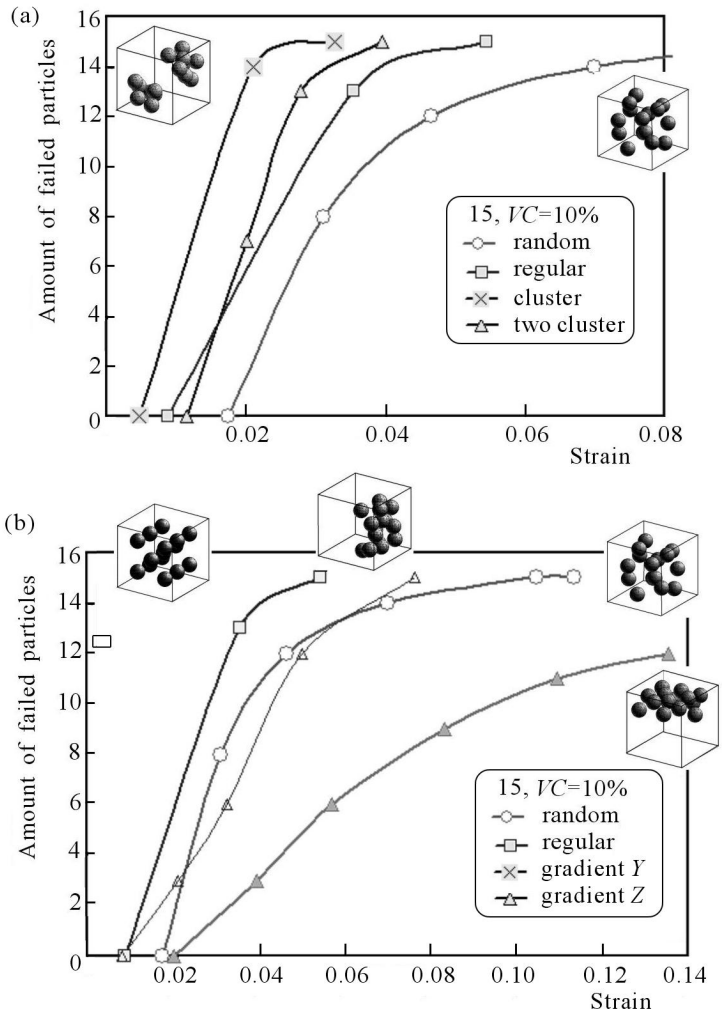

Fig. 4. Tensile stress-strain curves and the amount of failed particles in the box plotted versus the far-field applied strain for random, regular, clustered and gradient microstructures (for 15 particles, $VC = 10\%$)

response of the material becomes significant only at the load at which the particles begin to fail. However, after the particle failure begins, the effect of particle arrangement increases with the increasing load.

After the first particle fails, the flow stress of the composite increases with varying arrangement particle in the following order: gradient < random < clustered < regular microstructure. One can see in Fig. 4 that the rate of damage growth increases in the following order: gradient < random < regular < clustered.

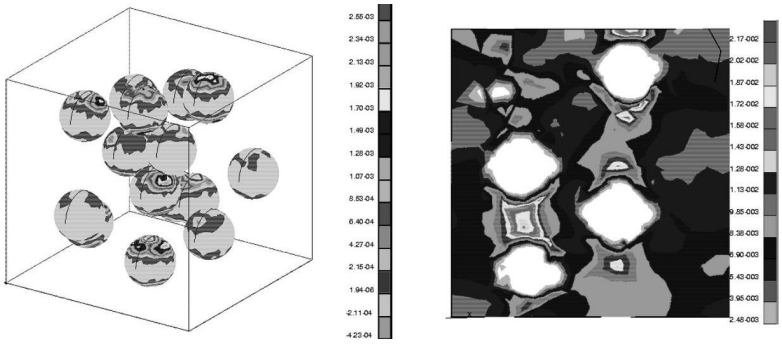

Fig. 5. Distributions of equivalent plastic strains on particle/matrix interfaces and in a vertical section in microstructures with random particle arrangements (15 particles, $VC = 10\%$)

The strength and damage resistance of a composite with a gradient microstructure strongly depends on the orientation of the gradient in relation to the direction of loading. In the case of a microstructure with the vertical gradient (along the loading vector), the rate of particle failure is very low (about 6.35 particle/mm) and the particle failure begins at a relatively high displacement loading, 0.2 mm. In the case of a microstructure with the horizontal gradient (normal to the loading vector), the rate of particle failure is the same as for random microstructures.

3.2. Damage evolution in graded composites and the effect of the degree of gradient

In the previous Section, it was shown that graded microstructures of composites ensure the highest damage resistance among all the considered microstructures. In this Section, we analyse the effect of the degree of particle localization in graded composites on their damage resistance. Here, we use a 2D version of the program "Meso3D" and 2D FE analysis.

As discussed above, the gradient degree of particle arrangement is determined by the standard deviation of the normal probability distribution of distances between the Y-coordinates of particle centers and of the upper boundary of the cell. Since the X-coordinates of particles are generated from a pre-defined random number seed parameter (idum) (which should ensure reproducibility of simulations), variations of this parameter lead to the generation of new realizations of microstructures with the same gradient. Many graded microstructures with different standard deviations of the distributions of Y-coordinates (which ensured different gradient degrees) and with different

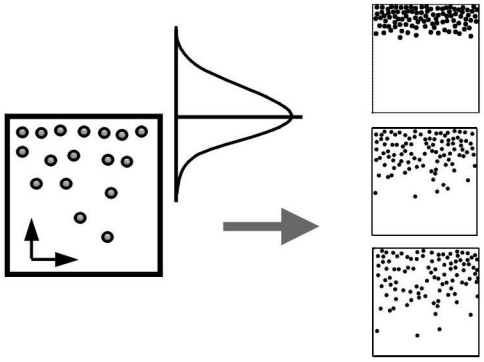

Fig. 6. Schema of design of artificial gradient microstructures and some examples of generated microstructures with different degrees of gradient

random number seed parameters for random X coordinates were generated, meshed and tested. Figure 7 shows some typical tensile stress-strain curves and the fraction of failed elements in the particles plotted versus the far-field applied strain for graded particle arrangements with different degrees of gradient.

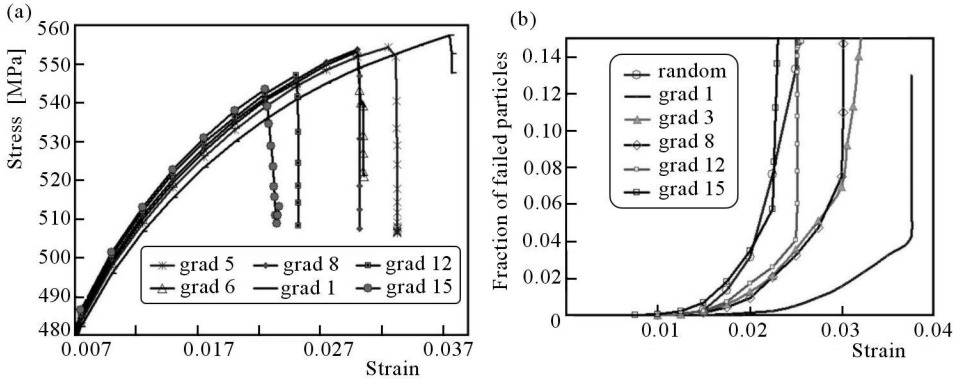

Fig. 7. Tensile stress-strain curves (a) and the fraction of failed elements in the particles plotted versus the far-field strain (b) for graded particle arrangements with different degrees of gradient

Figure 8a shows the failure strain (critical applied strain) plotted versus the degree of gradient in the composites. Figure 8b shows the flow stress of the composite (at the far-field strain $u = 0.15$) as a function of the gradient degree.

It is of our interest that the flow stress and stiffness of composites decrease with the increasing degree of gradient. Apparently, the more homogeneous is

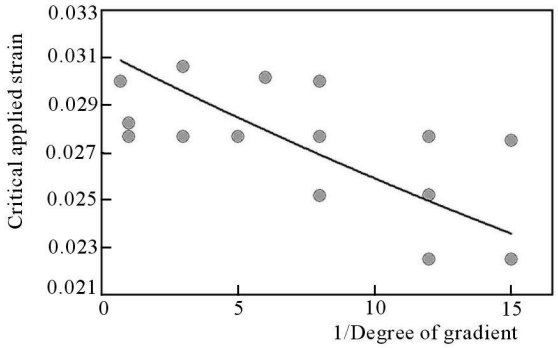

Fig. 8. Failure strain of the composite (at the far-field strain $u = 0.15$) plotted versus the degree of gradient in the composites

the distribution of hard inclusions in the matrix, the stiffer is the composite. If the particles are localized in one layer in the composite, the regions with low particle density determine the deformation of the material, and that leads to a low stiffness.

One can see in Fig. 7b that all microstructures have rather low damage growth rate at the initial stage of damage evolution. At some far-field strain (called here "failure strain"), the intensive (almost vertical) damage growth takes place and the falling branch of the stress-strain curve begins. For all the graded microstructures, the failure strain is higher than for the homogeneous microstructures. The failure strain of composites increases with the increasing gradient degree.

Figure 9 shows von Mises stress distribution in a highly gradient (grad3) microstructure. One can see that the stresses are lower in the low part of the microstructure (particle-free region) than in the particle-rich regions. If two particles are placed very closely one to another, the stress level in the particles is much higher than in other particles, especially if these particles are arranged along the gradient (vertical) vector. Then, the stress level is rather high in particles which are located in the transition region between the high particle density and particle-free regions. One could expect that these particles begin to fail at later stages of loading, and that was observed in damage simulations indeed.

Figure 9b shows damage distribution in the particles and in the matrix (grad3 microstructure, far-field strain 0.29). The fact that the particles begin to fail not in the region of high particle density but rather in the transition region between the particle-rich and particle-free regions is similar to our observations for the case of the clustered particle arrangement, where the damage

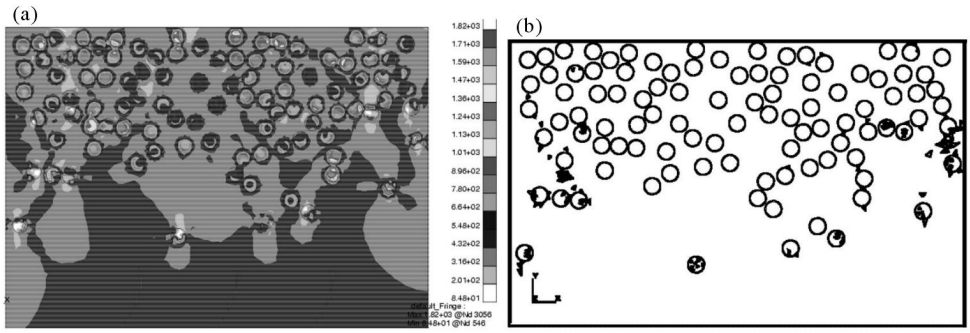

Fig. 9. Von Mises stress distribution in a highly gradient (grad3) microstructure (a) and damage distribution in the particles and in the matrix (grad3 microstructure, far-field strain 0.29)

begins in particles which are placed at the outer boundaries of clusters (Mishnaevsky *et al.*, 2004a). One can see in Fig. 9b that the damage in the matrix begins near the damaged particles or between particles which are arranged closely in the direction of the gradient vector.

3.3. Effect of sharpness of the transition region in graded composites

In this Section, we analyse the effect of sharpness of the transition region between phases in graded composites on strength and stiffness of composites. To do it, we use the program "Voxel2FEM", described in Section 2.2, which allows us to vary the sharpness of the transition region.

The 3D unit cell models of graded composites with varied sharpness/smoothness of the transition region between phases were generated as follows. The unit cells were considered as consisting of voxels (points) of white (matrix) and black (particles) phases. The distribution of black voxels was defined as random distributions in the X and Z directions and a graded distribution in the Y direction. The graded distribution of black voxels (e.g., grains of hard phase) along the axis Y follows the formula

$$vc(y) = \frac{2vc_0}{1 + \exp\left(g - \frac{2gy}{L}\right)} \tag{3.1}$$

Here $vc(y)$ is the probability that a voxel is black at a given point, vc_0 is the volume content of the black phase, L denotes the length of the cell, g is a parameter of the gradient, y is the Y-coordinate. Equation (3.1) allows one to vary the smoothness of the gradient interface of the structures (highly localized arrangements of inclusions and a sharp interface versus a smooth interface),

keeping the volume content of the inclusions constant. If $g < 3$, the transition between the regions of high content of black or white phases is rather smooth, and if $g > 10$, the transition between the regions is rather sharp. Figure 10 gives shapes of this curve for different g. Figure 11 gives examples of such microstructures.

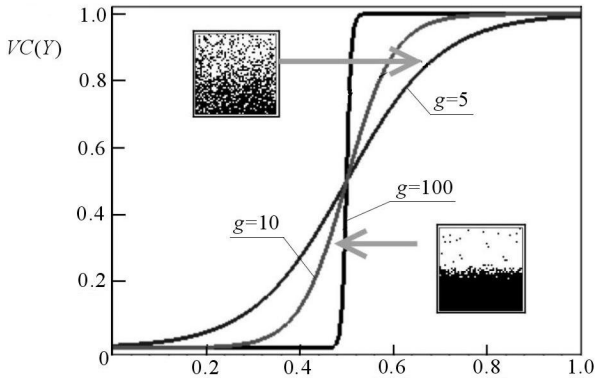

Fig. 10. Shapes of the curve which describes transition between the regions of high content of different phases for different parameters g ($g = 5$, 10, 100, $vc = 50\%$) (Mishnaevsky, 2005); y denotes Y-coordinate, L is the linear size of the cell

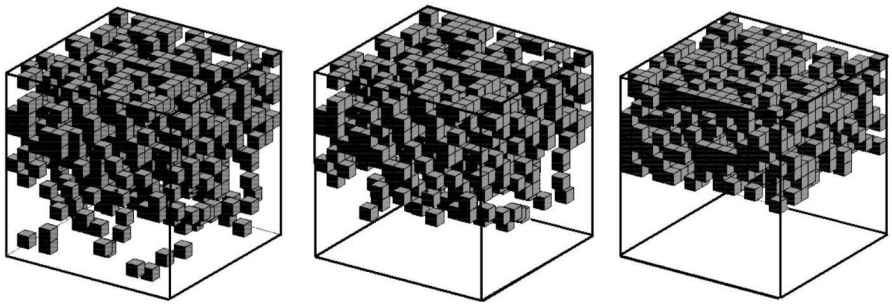

Fig. 11. Examples of the considered graded microstructures of the material: $g = 3$, $g = 6$, $g = 100$

Figure 12 shows stress-strain curves of composites with a volume content of the hard phase 10% and 20%, and with a varied gradient parameter g, Eq. (3.1). Observing the curves, one can see that the critical strain, at which damage growth begins, does not depend on the parameter of the volume fraction gradient g. Whether the transition between the region of high content of the hard phase to the region of low content is sharp or smooth, the critical applied strain remains constant. However, the stiffness of the composite and

the peak stress of the stress-strain curve increase with increasing sharpness of the transition between the regions. A reduction of the value g from 20 to 1 can lead to a decrease in the peak stress by 6%.

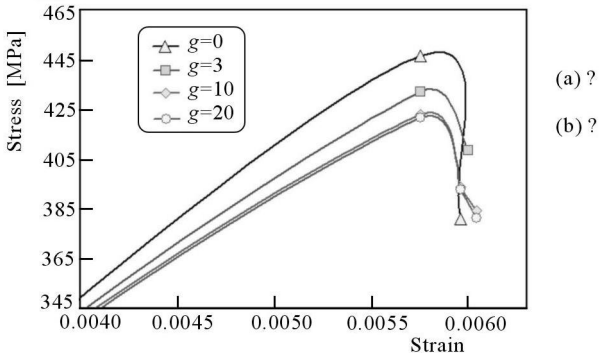

Fig. 12. Typical tensile stress-strain curves for different sharpness of transition zones of graded composites: (a) $VC = 10\%$, (b) $VC = 20\%$ (Mishnaevsky, 2005)

Figure 13 shows the peak stress of the stress-strain curve plotted versus the parameter g of the transition of sharpness between the regions of high and low content of the hard phase.

Comparing this conclusion with the results from Sections 3.1 and 3.2, one may summarize that Al/SiC graded composites with a high gradient degree and smooth transition between the region with a high content of the SiC phase and the reinforcement-free region can ensure both highest damage resistance and a relatively high stiffness.

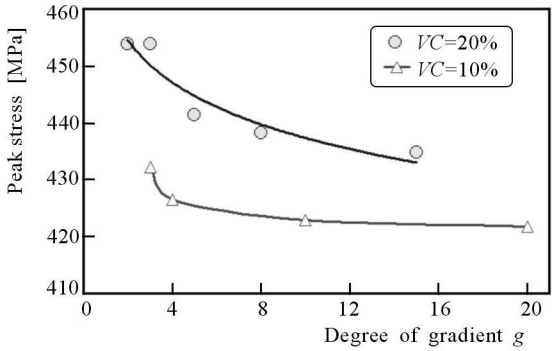

Fig. 13. Peak stresses of the stress-strain curve plotted versus sharpness of the transition zone for graded composites with different volume content of the hard phase (10% and 20%) (Mishnaevsky, 2005)

3.4. Mesomechanical simulation of wear of diamond grinding wheels

In this Section, the methods of computational mesomechanics were used to analyse mechanical wear of diamond grinding wheels in grinding. We consider here straight grinding wheels with synthetic diamonds and bronze copper bond (which are used for grinding ceramics, for instance). 3D FE models of cutouts of the work surface of a grinding wheel have been generated automatically using the program "Meso3D" (Section 2.1). On the contact surface 10×10 mm, 15 diamond grains were randomly placed. The radius of grains was 1.16 mm (therefore, 63% of the contact surface was taken by the diamond grains).

The material properties were as follows: diamond: Young's modulus $E = 900$ GPa, Poisson's ratio $\nu = 0.2$, compressive yield strength 5 MPa; bond: $E = 93$ GPa, tensile yield stress 125 MPa, yield strain 0.2%, ultimate tensile strength 255 MPa (Bauccio, 1994). The failure stress of the diamond grains was assumed to be 20 GPa (Mishnaevsky, 1982). The grain tips have been loaded by an inclined force, 70 N/grain. The force was oriented at 60° angle to the horizontal line. The temperature effect was neglected in the first approximation, following the results by Mishnaevsky (1982), which demonstrated that the local heating up to 200-300°C (i.e., local temperatures observed on grain surfaces at relatively low cutting speeds) does not change the mechanisms and critical parameters of grain destruction. The damage in the diamond grains was modeled using the subroutine User Defined Field, presented in Section 3.1, and the element weakening approach. The critical maximum stress was taken as the criterion of the finite element failure.

Figure 14 shows the von Mises strain distribution in the diamond grains and in the metal bond in grinding (a) and the fraction of failed elements in the grains plotted versus the applied force (b).

One can see in Figure 14 that high strains are localized near the peaks of the diamond grains. This corresponds to experimental observations in Mishnaevsky (1982): damage in diamond grains in grinding is observed in a small region near the grain peak. It can be seen in Figure 14b that the damage growth starts at the force 24 N and becomes very intensive at about 45 N.

The results presented in this section demonstrate the applicability of the computational mesomechanics approach and the numerical tools developed above to analysis of wear of diamond grinding wheels.

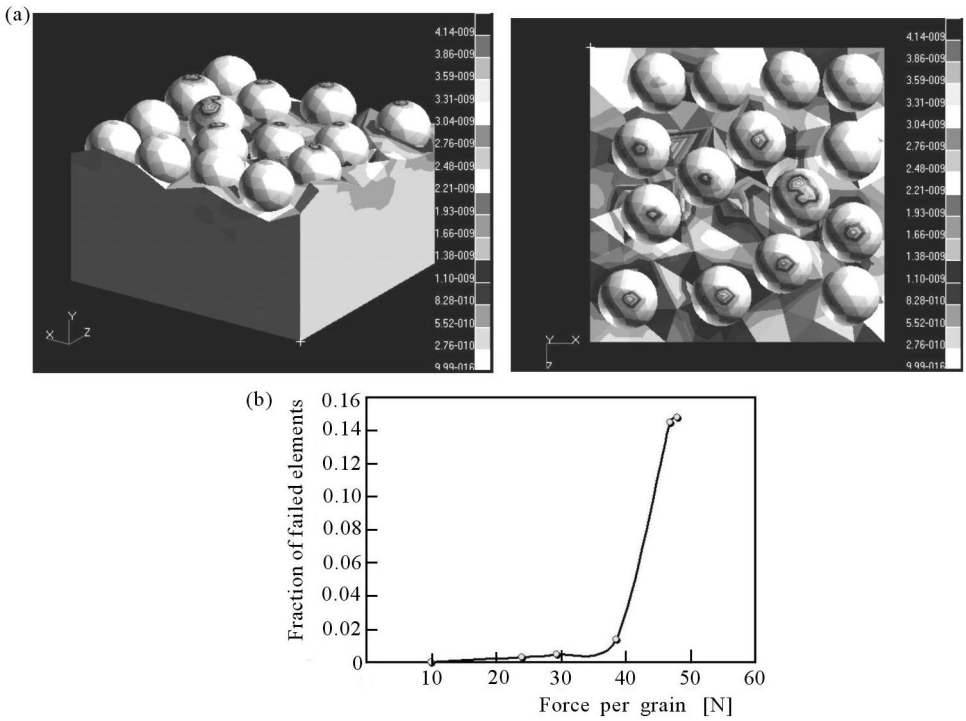

Fig. 14. Von Mises strain distribution in diamond grains and in the metal bond of a grinding wheel (a) and the fraction of failed elements in the diamond grains plotted versus the applied force (b)

4. Conclusions

Numerical investigations of the effect of a microstructure, arrangement and volume content of hard damageable inclusions in a plastic matrix on the deformation and damage growth are presented in the paper. It was shown that the flow stress of a composite increases with the particle arrangement varying in the following order: highly gradient < random < clustered < regular microstructure. The rate of damage growth increases in the following order: gradient < random < regular < clustered. The flow stress and stiffness of composites decrease with the increasing gradient degree, whereas the failure strain increases with the increasing gradient degree of the particle arrangement. More localized and highly gradient microstructures have lower stiffnesses and higher failure strains than homogeneous microstructures. It was shown that the stiffness of a composite and the peak stress of the stress-strain curve increase

with increasing smoothness of the transition between the region of a high volume content of the hard phase to the region of a low content of the hard phase.

Acknowledgement

The author is grateful to the German Research Council (DFG) for its support through the Heisenberg fellowship.

References

1. BAUCCIO M., EDIT., 1994, *ASM Engineered Materials Reference Book*, 2nd Ed., ASM International, Materials Park, OH
2. DERRIEN K., BAPTISTE D., GUEDRA-DEGEORGES D., FOULQUIER J., 1999, Multiscale modelling of the damaged plastic behaviour of AlSiCp composites, *Int. J. Plasticity*, **15**, 667-685
3. MISHNAEVSKY L. JR., 1998, *Damage and Fracture of Heterogeneous Materials*, Balkema, Rotterdam, 230 pp.
4. MISHNAEVSKY L. JR., 2004, Three-dimensional numerical testing of microstructures of particle reinforced composites, *Acta Mater.*, **52**, 14, 4177-4188
5. MISHNAEVSKY L. JR., 2005, Automatic voxel based generation of 3D microstructural FE models and its application to the damage analysis of composites, *Materials Science and Engineering*, **A 407**, 1/2, 11-23
6. MISHNAEVSKY L. JR., DERRIEN K., BAPTISTE D., 2004a, Effect of microstructures of particle reinforced composites on the damage evolution: probabilistic and numerical analysis, *Composites Science and Technology*, **64**, 12, 1805-1818
7. MISHNAEVSKY L. JR., DONG M., HOENLE S., SCHMAUDER S., 1999a, Computational mesomechanics of particle-reinforced composites, *Comput. Mater. Sci.*, **16**, 1/4, 133-143
8. MISHNAEVSKY L. JR., LIPPMANN N., SCHMAUDER S., 2003a, Computational modeling of crack propagation in real microstructures of steels and virtual testing of artificially designed materials, *Int. J. Fracture*, **120**, 4, 581-600
9. MISHNAEVSKY L. JR., LIPPMANN N., SCHMAUDER S., 2003b, Micromechanisms and modelling of crack initiation and growth in tool steels: role of primary carbides, *Zeitschrift f. Metallkunde*, **94**, 6, 676-681
10. MISHNAEVSKY L. JR., LIPPMANN N., SCHMAUDER S., GUMBSCH P., 1999b, In-situ observations of damage evolution and fracture in AlSi cast alloys, *Eng. Fract. Mech.*, **63**, 4, 395-411

11. MISHNAEVSKY L. JR., SCHMAUDER S., 2001, Continuum mesomechanical finite element modeling in materials development: a state-of-the-art review, *Applied Mechanics Reviews*, **54**, 1, 49-69

12. MISHNAEVSKY L. JR., WEBER U., SCHMAUDER S., 2004b, Numerical analysis of the effect of microstructures of particle-reinforced metallic materials on the crack growth and fracture resistance, *Int. J. Fracture*, **125**, 33-50

13. MISHNAEVSKY L.L., 1982, *Wear of Grinding Wheels*, Kiev, Naukova Dumka

14. MUMMERY P., DERBY B., 1993, In: *Chapter 14, Fundamentals of Metal-Matrix Composites*, S. Suresh, A. Mortensen, A. Needleman (edit.), Elsevier, 251-268

15. RICE J.R., TRACEY D.M., 1969, On the ductile enlargement of voids in triaxial stress fields, *Int. J. Mech. Phys. Solids*, **17**, 201-217

16. WULF J., 1995, Neue Finite-Elemente-Methode zur Simulation des Duktilbruchs in Al/SiC, Dissertation MPI für Metallforschung, Stuttgart

17. WULF J., SCHMAUDER S., FISCHMEISTER H.F., 1993, Finite element modelling of crack propagation in ductile fracture, *Comput. Mater. Sci.*, **1**, 297-301

Wpływ mikrostruktury na zniszczenie kompozytu – analiza numeryczna

Streszczenie

W artykule przedstawiono analizę wpływu mikrostruktury materiałów kompozytowych na ich odporność na zniszczenie, przeprowadzając badania symulacyjne oparte na modelach obliczeniowych stosowanych w mezo-mechanice oraz na eksperymentach numerycznych. Opisano zaproponowane i przetestowane programy do automatycznego generowania trójwymiarowych modeli mikkrostruktur kompozytowych bazujące na opisie geometrycznym z zastosowaniem techniki wokseli (3-wymiarowych odpowiedników pikseli). Przeprowadzono symulacje deformacji i ewolucji zniszczenia elementów skończonych reprezentujących kompozyty z wtrąceniami punktowymi o różnej mikrostrukturze. Sformułowano pewne wytyczne dla poprawy odporności na zniszczenia lekkich kompozytów zbudowanych z metalicznego lepiszcza wzmacnianego ceramiką.

Manuscript received December 24, 2005; accepted for print January 11, 2006